JCTC Journal of Chemical Theory and Computation

Article

pubs.acs.org/JCTC

Reaction Path Following with Sparse Interpolation

James Nance,[†] Elena Jakubikova,[‡] and C. T. Kelley*,[†]

[†]Department of Mathematics and [‡]Department of Chemsitry, North Carolina State University, Raleigh, North Carolina, United States

Supporting Information

ABSTRACT: Computing the potential energy of an N-atom molecule is an expensive optimization process of $3N - 6$ molecular coordinates, so following reaction pathways as a function of all $3N - 6$ coordinates is unfeasible for large molecules. In this paper, we present a method that isolates $d < 3N - 6$ molecular coordinates and continuously follows reaction paths on d-dimensional potential energy surfaces approximated by a Smolyak's sparse grid interpolation algorithm.[1] Compared to dense grids, sparse grids efficiently improve the ratio of invested storage and computing time to approximation accuracy and thus allow one to increase the number of coordinates d in molecular reaction path following simulations. Furthermore, evaluation of the interpolant is much less expensive than the evaluation of the actual energy function, so our technique offers a computationally efficient way to simulate reaction paths on ground and excited state potential energy surfaces. To demonstrate the capabilities of our method, we present simulation results for the isomerization of 2-butene with two, three, and six degrees of freedom.

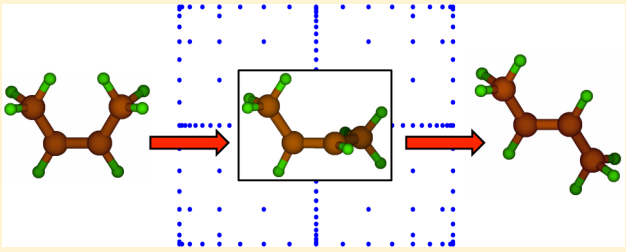

1. INTRODUCTION

The potential energy surface of a molecule describes the energy of an N-atom molecule as a function of its $3N - 6$ geometric coordinates.[2] Local minima of these surfaces correspond to stable molecular geometries, and first order saddle points correspond to transition states. As such, there is great interest in studying the global structure of these potential energy surfaces. Methods for potential energy surface exploration include: the Hills method,[3−5] the scaled hypersphere method,[6−9] the fast-marching method,[10−14] and conformational flooding.[15,16] Knowledge of the potential energy surface landscape is necessary to follow reaction paths from stable molecular conformations to transition states or other stable conformations.[17−28]

Molecules of interest can have hundreds of atoms and degrees of freedom, so exploring potential energy surfaces and simulating reactions continuously can be computationally burdensome. Furthermore, most of these methods are restricted to the ground state potential energy surface and only provide partial reaction or conformation paths. In this paper, we present a new method for calculating potential energy surfaces and following continuous steepest descent reaction paths between stable ground state conformations via excited state transitions.

The simulation of excited state dynamics can be separated into two areas: adiabatic dynamics and nonadiabatic dynamics. Much recent work has been focused on the latter for the theoretical study of ultrafast photochemical processes,[26,29−32] for example. The most popular approach for treating nonadiabatic effects of such processes is the surface hopping method[29,33−38] where nuclei move on a single potential energy surface and trajectories are allowed to hop from one surface to another. Surface hopping is often employed in the hybrid quantum-mechanical/molecular-mechanical (QM/MM) context[39] that treats a small part of the system at an appropriate quantum mechanical level and treats the rest with a cheaper molecular mechanical force field. Steepest descent paths have also been studied in the QM/MM regime.[26,40−44]

Other work on following pathways on nonadiabatic potential energy surfaces includes: the semiclassical electron-radiation-ion dynamics (SERID) method[31,32,45,46] the multiconfiguration molecular mechanics method,[47−52] and the ab initio multiple spawning (AIMS) method.[53−55] Barbatti and co-workers have recently developed the robust software package Newton-X[56,57] for nonadiabatic (and adiabatic) simulations. Finally, extensive reviews of recent advances in the field of direct nonadiabatic simulations can be found in refs 58 and 59.

While these direct methods are very accurate, they require many expensive electronic structure calculations during dynamics simulations. The method proposed in this paper is advantageous in that it requires no electronic structure calculations during the simulation. All necessary electronic structure calculations are computed a priori before dynamics are initialized. Furthermore, these calculations are independent and can be computed in parallel.

The method proposed here constructs global *adiabatic* potential energy surfaces by means of interpolation. Spline interpolation has been used to construct global potential energy surfaces for $d \leq 3$ dimensions[60−62] and has recently been applied to higher dimensions with nonuniform meshes.[63] These interpolation methods, however, are restricted to small

Received: February 24, 2014
Published: July 2, 2014

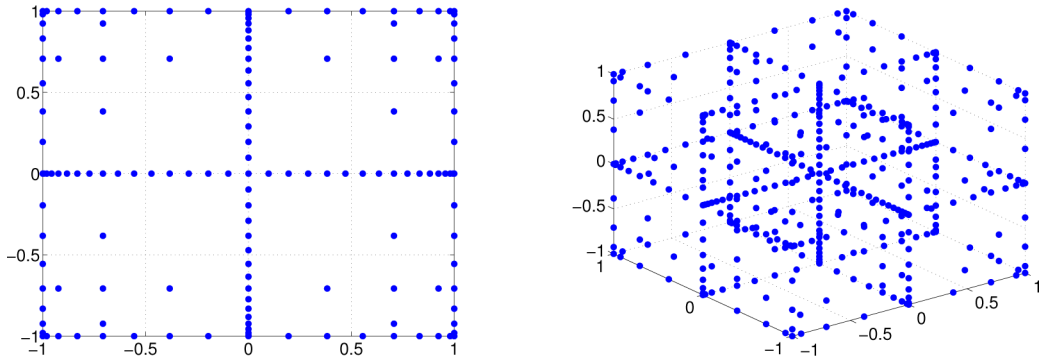

Figure 1. Sparse grids for $\mathcal{H}(7, 2)$ (left) and $\mathcal{H}(8, 3)$ (right) on the domains $[-1, 1]^2$ and $[-1, 1]^3$, respectively.

molecules because of the computational cost of constructing the potential energy surfaces to within a sufficient accuracy. The number of grid points required for interpolation on full grids grows exponentially with dimension, a problem known as the *curse of dimensionality*. Other more local potential energy surface exploration methods include schemes based on modified Shepard interpolation,[64−66] moving least-squares,[67,68] and combinations thereof.[11] Our global method, however, is better suited for exploring reaction paths of molecules that have several local minima. As detailed later, our method is capable of following several trajectories simultaneously and can identify local minima that the aforementioned local methods may not detect. While we may perform electronic structure calculations in areas of the grid that are not visited by simulation trajectories, the calculations still contribute by decreasing the interpolation error of our approximation and are therefore not superfluous.

The method for reaction path following presented here is based on the work of Mokrauer, Kelley, and Bykhovski[62,69−72] that follows reaction paths on surrogate potential energy surfaces approximated by interpolation on sparse grids.[1,73,74] Sparse grids have been applied to quantum chemistry before to solve the Schrödinger equation,[75−83] but our application differs from previous work in that we treat electronic structure calculations as a black box function that we aim to interpolate.

Compared to full grids, sparse grids efficiently improve the ratio of invested storage and computing time to approximation accuracy. A key advantage of kind of sparse grids we employ is that the number of nodes required for interpolation grows only polynomially with dimension.[84] Therefore, sparse interpolation overcomes the curse of dimensionality to some extent and thus increases the number of dimensions one can explore on the potential energy surface. Bungartz and Griebel present a wonderful review of sparse grids in ref 85, and the interested reader is referred there for a more thorough introduction to the subject.

For many reactions, only a handful of the $3N - 6$ molecular coordinates change significantly and the rest remain approximately constant. As such, a popular approach is to follow reaction paths for only a small subset of the $3N - 6$ molecular coordinates. Mokrauer's approach isolates a few, say d, molecular coordinates and then uses sparse interpolation to approximate the potential energy surfaces in patches during the reaction simulation using a combination of trust-region and error estimation algorithms.[72] The numerous interpolation patches, however, introduce discontinuities in the potential energy surface that are unphysical. The method presented in this paper is similar but constructs a single global potential energy surface and then simulates the reaction. In this way, one can visualize the entire potential energy surface landscape before simulating the reaction process. Furthermore, this new reaction path following method allows one to track entire reaction paths on the ground and all specified excited state potential energy surfaces. Knowledge of excited state dynamics is particularly useful in studying reaction paths of isomerization processes, for example.

The rest of this paper is outlined as follows: in section 2, we describe a surrogate model for reaction path following using sparse interpolation. In section 3, we present simulation results for the isomerization of 2-butene, and we conclude in section 4.

2. METHODOLOGY

2.1. Potential Energy Surface Approximation. In this section, we describe how we approximate potential energy surfaces using a sparse grid interpolation algorithm developed by Smolyak.[1,73,74] The potential energy E_n of an N-atom molecule at any electronic state $n = 0,1,2,...$ can be computed as a function of (redundant) internal coordinates $\mathbf{p} \in \mathbb{R}^{3N-6}$ composed of bond lengths, bond angles, and dihedral angles. The first step of our method is to partition $\mathbf{p} = (\mathbf{x}, \boldsymbol{\xi})$ into a vector of design variables $\mathbf{x} \in \mathbb{R}^d$ and a vector of remainder variables $\xi \in \mathbb{R}^{3N-6-d}$, where chemical knowledge or intuition of the system guides the appropriate choice of design variables $\mathbf{x}$. The d-dimensional ground state potential energy surface is computed via the constrained optimization problem

$$E_0(\mathbf{x}) = \min_{\xi} \mathcal{E}_0(\mathbf{x}, \xi) \tag{1}$$

where the minimization is only over the remainder variables $\boldsymbol{\xi}$. Points on the excited state potential energy surfaces $E_n(\mathbf{x})$, $n \geq 1$, are calculated at optimized ground state geometries. Because eq 1 is such an expensive optimization process, continuous dynamical simulations are often unfeasible. Smolyak's algorithm,[1,73,74] however, allows one to simulate dynamics with a cheap surrogate potential energy function.

2.1.1. Smolyak's Algorithm. Smolyak's interpolation algorithm constructs an interpolating polynomial from a linear combination of interpolating polynomials on different "levels" of grids. Given a polynomial degree of exactness k, dimension d, and domain for interpolation, the algorithm constructs an interpolating polynomial via the functional

$$\mathcal{A}(q, d) = \sum_{\mathbf{i} \in Q(q,d)} (-1)^{q-|\mathbf{i}|} \binom{d-1}{q-|\mathbf{i}|} \mathbf{U}^{\mathbf{i}} \tag{2}$$

dx.doi.org/10.1021/ct5004669 | J. Chem. Theory Comput. 2014, 10, 2942−2949

where $q = d + k$, $\mathbf{U}^{\mathbf{i}}$ is a tensor product of Lagrange basis polynomials, and the multi-index $\mathbf{i}$ encodes the level of grid for each term of the linear combination. The mathematical details of Smolyak's algorithm are tedious and are omitted here for simplicity, but the interested reader can find them in refs 1, 73, and 74, or in the Supporting Information to this paper. Instead, we highlight a few key features of the method that make it appealing to reaction path following.

First, the sparse grid points used in Smolyak's algorithm, which we denote by $\mathcal{H}(q, d)$, are uniquely specified by d, k, and the interpolation domain. We use sparse grids with Chebyshev nodes as first proposed for interpolation in ref 73. Smolyak's interpolating polynomial is constructed by evaluating the function $f(x)$ at each point of the sparse grid. Figure 1 shows two Chebyshev sparse grids: the first is the two-dimensional sparse grid $\mathcal{H}(7, 2)$ on the domain $[-1, 1]^2$, and the second is the three-dimensional sparse grid $\mathcal{H}(8, 3)$ on $[-1, 1]^3$. We note that the interpolation domain for the ith dimension must be specified to match the corresponding design variable x_i. For example, $[0°, 360°]$ would be an appropriate domain for a dihedral angle.

Second, sparse grids are nested in k, that is, $\mathcal{H}(q, d) \subset \mathcal{H}(q + 1, d)$. This means that one can reuse all of the function evaluations from the k sparse grid, which are in our case expensive electronic structure calculations, to obtain an approximation on the $k + 1$ sparse grid. The nestedness also allows one to estimate interpolation errors.[71] Explicit error bounds for Smolyak's algorithm have been studied extensively,[1,73,84,86] but in general, they depend on the dimension d, the degree of polynomial exactness k, the size of the interpolation domain, and the smoothness of the potential energy surfaces $E_n(\mathbf{x})$. We note that one must take care in choosing an appropriate interpolation domain. If the molecular geometry at a point in the domain is undefined, for example, if two nuclei are at the same position, the error bounds derived in ref 73 do not hold. One should in general ensure that the potential energy surfaces are bounded by choosing arbitrary but finite bounds for bond lengths and by choosing bounds for bond angles and torsional angles that do not yield unphysical geometries. Finally, the number of sparse grid points for a fixed k grows only polynomially with dimension instead of exponentially.[84] To illustrate this drastic reduction in grid points, Table 1 compares the number of grid points needed for tensor product interpolation with five points in each dimension and Smolyak's sparse grid interpolation.

To employ Smolyak's algorithm one must perform the electronic structure optimization in eq 1 and any corresponding excited state energy calculations for each point $\mathbf{x}_i$ in the sparse grid $\mathcal{H}(q, d)$. While the necessary electronic structure calculations are expensive, they are the sole computational burden of this method. With the sets of sparse grid points $\mathbf{x}_i$ and energy values $E_n(\mathbf{x}_i)$ in hand, one can use eq 2 to interpolate the potential energy surfaces. We will denote this surrogate for the potential energy function by

$$E_n^s(\mathbf{x}) = \mathcal{A}(q, d)[E_n](\mathbf{x}) \tag{3}$$

for any electronic state $n \geq 0$.

Table 1. Number of Grid Points for Tensor Product Grids with Five Points in Each Dimension and for Smolyak Sparse Grids

		sparse grid		
d	tensor product	$k = 1$	$k = 2$	$k = 3$
1	5	3	5	9
2	25	5	13	29
5	3125	11	61	241
10	9 765 625	21	221	1581

2.2. Reaction Path Dynamics. The goal of our simulations is to successfully predict the natural excitation and relaxation of a molecule for a given sequence of m electronic states $\{n_1, ..., n_m\}$ and track the entire reaction path. The sequence can specify both multiphoton and single photon excitations, as well as any decay path. For example, a sequence of $\{0, 3, 0\}$ would represent a single photon excitation and relaxation between the ground state and the third excited state. The reaction path of a molecule moves in the direction of the negative gradient on potential energy surfaces,[87] and large steps across the potential energy surfaces may pass over local minima or be physically unnatural. With this in mind, we track the reaction path and find local minima via continuous steepest descent[88,89] by integrating the dynamics

$$\dot{\mathbf{x}} = -\nabla E_n^s(\mathbf{x}) \tag{4}$$

until $\|\nabla E_n^s(\mathbf{x})\|$ is smaller than a prescribed tolerance $\tau \approx 0$.

The solution $\mathbf{x}$ to eq 4 is the reaction path and is approximated using MATLAB's ode15s variable order solver.[90,91] We stress that the time step is nonphysical and in no way reflects the time scale of the physical reaction; we are only interested in the path the molecule takes. Continuous steepest descent would be unfeasible without the surrogate model. The gradient of the potential energy in eq 1, while available in analytic form, is far too expensive to compute at each time step. On the other hand, the surrogate model $E_n^s(\mathbf{x})$ and its gradient, which can also be computed analytically, are both multidimensional polynomials and are much less expensive to evaluate than $E_n(\mathbf{x})$ and its gradient $\nabla E_n(\mathbf{x})$. For moderately sized molecules, the evaluation time can be reduced from several minutes to a fraction of a second.

Each reaction path simulation begins with $n_1 = 0$ at an equilibrium geometry on the surrogate ground state potential energy surface, from which the molecule is excited to the next specified electronic state n_2. The steepest descent path is followed to find a local minimizer $\hat{\mathbf{x}}^{n_2}$ on the potential energy surface, and then the molecule is excited to the next state. The simulation continues in this way until a local minimum on the highest specified electronic state, say n_i, has been reached. To simulate the relaxation of a molecule from one state to the next, thermal fluctuations and molecular vibrations are accounted for by reinitializing dynamics on the succeeding state at $\hat{\mathbf{x}}^{n_i} + \gamma$ where γ is a d-dimensional vector of random numbers. The domain for γ_j depends on the type of molecular coordinate: $\gamma_j \in [-0.025, 0.025]$ if the jth design variable is a bond length, and $\gamma_j \in [-30, 30]$ if the jth design variable is a bond or dihedral angle. These intervals were chosen arbitrarily to approximate the effects of molecular vibrations and thermal fluctuations.

3. EXAMPLE

A good test molecule for our simulations is 2-butene because it has a known transition path from *cis*-2-butene to *trans*-2-butene via excitation to the first excited singlet state.[62,71,92−96] Both

stable ground state geometries for 2-butene are shown in Figure 2 where we label each of the four C atoms with superscripts.

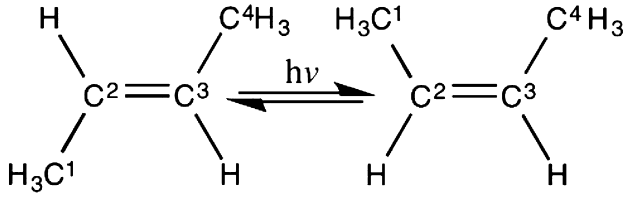

Figure 2. Photoisomerization of *trans*-2-butene (left) and *cis*-2-butene (right). Carbon atoms are labeled with superscripts.

3.1. Computational Details. The first step of our reaction path method is to choose design coordinates and corresponding interpolation bounds. The main reaction coordinate for the isomerization of 2-butene is the dihedral angle formed by the four C atoms $C^1—C^2═C^3—C^4$, so we choose this angle to be x_1. The *cis*-2-butene and *trans*-2-butene geometries correspond to $x_1 = 0°$ and $x_1 = 180°$ and the transition state corresponds to $x_1 = 90°$, so we choose bounds of $[-20, 200]$ degrees for x_1. The second and third coordinates x_2 and x_3 are rotations of the methyl groups that are governed by the dihedral angles formed by the atoms $C^3═C^2—C^1—H_3$ and $C^2═C^3—C^4—H_3$. Only one C═C—C—H dihedral angle is frozen during the optimization, as we expect the methyl group to retain its symmetry. We do not expect these coordinates to change much during the simulation, so we choose bounds of $[-100, 100]$ degrees for both x_2 and x_3. Design coordinates x_1, x_2, and x_3 are shown in Figure 3. Finally, we choose the three carbon−carbon

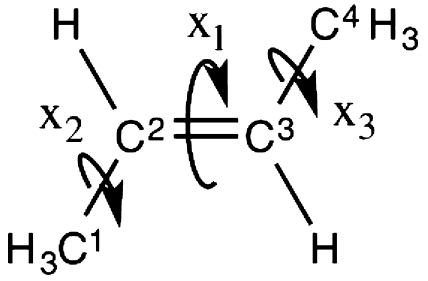

Figure 3. Design variables x_1, x_2, and x_3 for 2-butene simulations.

bond lengths as additional degrees of freedom. The $C^2═C^3$ bond length is x_4, the $C^1—C^2$ bond length is x_5, and $C^3—C^4$ bond length is x_6. The interpolation domain for each of these bond length coordinates is $[1.3, 1.7]$ Å.

We know that the isomerization takes place via the first excited state,[96] so our sequence of electronic states to model this phenomenon is $\{0, 1, 0\}$.

We present results for four simulations: simulation 1 is a two-dimensional simulation with design coordinates x_1 and x_2 and degree of exactness $k = 4$, and simulation 2 is the same as simulation 1 but with $k = 5$. Simulation 3 is a three-dimensional simulation with design coordinates x_1, x_2, and x_3 and a degree of exactness of $k = 5$. Simulation 4 is a six-dimensional simulation with all six design coordinates and a degree of exactness of $k = 5$. To our knowledge, this is the first time 2-butene isomerization has been studied with more than three degrees of freedom.

While our method can be applied using any electronic structure method and basis set, each geometry optimization for the first three simulations is calculated using the B3LYP hybrid functional[97,98] with the CEP-31G* basis set.[99−101] For the fourth simulation, the molecule's geometry is optimized at the B3LYP/3-21G* level of theory and then the energy is computed at the B3LYP/CEP-31G* level of theory at the optimized geometry. All excitation energies are computed using the TD-DFT method.[102] We used the *GAUSSIAN 09* software package[103] for all electronic structure calculations.

All four simulations are initialized at the stable *cis*-2-butene geometry, and the gradient norm tolerance for continuous steepest descent is set to $\tau = 10^{-10}$. We employ our own implementation of Smolyak's algorithm that is specifically designed to construct and follow multiple dynamics paths on potential energy surfaces.[104] In the following, all units for reported energies, angles, and bond lengths are electronvolts (eV), degrees, and angstroms (Å), respectively.

3.2. Results. *3.2.1. Simulation 1: d = 2, k = 4.* The interpolated potential energy surfaces for both the ground and first excited state are shown in Figure 4A with each sparse grid point. One can visually observe that the global minimum of the first excited state lies directly above the global maximum of the ground state, so it is clear that randomness caused by molecular vibrations and thermal fluctuations could play an important role in the reaction. Also, as we expect, the potential energy does not vary much in the x_2 direction.

While the potential energy surfaces look appealing, local minima of the ground state are found to have x_1 values of 17.3 for *cis* and 166 for *trans*. It is known that x_1 should be either 0 or 180 at the stable geometries,[93,95,96] thus we must increase the accuracy of our approximated potential energy surfaces to improve our results. The nested structure of sparse grids allows us to reuse all of the electronic structure calculations from the $k = 4$ sparse grid to compute the $k = 5$ sparse grid. There are 65 grid points in $\mathcal{H}(6, 2)$ and 145 in $\mathcal{H}(7, 2)$, so we only need to perform 80 additional electronic structure calculations.

3.2.2. Simulation 2: d = 2, k = 5. With a higher degree of exactness, x_1 now has values of 1.48 for *cis* and 179 for *trans*, which we deem sufficient for our simulations. The reaction path is initialized on the ground state in the *cis* geometry at $\mathbf{x} = (1.48, -0.95)$, and continuous steepest descent converges to a minimizer of $\hat{\mathbf{x}}^1 = (92.9, -23.2)$ on the first excited state potential energy surface. Since this minimizer lies almost directly above the ground state transition state, the approximated effects of thermal fluctuations and molecular vibrations upon relaxation either send the molecule back to its original geometry or toward its *trans*-2-butene counterpart. The *trans* geometry is found to be $\mathbf{x} = (179, 2.42)$. Fifty different reaction paths are shown on the potential energy surfaces in Figure 4.

3.2.3. Simulation 3: d = 3, k = 5. For this simulation, we include our third degree of freedom x_3. The reaction path is initialized on the ground state at $\mathbf{x} = (1.16, -0.30, -0.30)$, corresponding to a *cis*-2-butene geometry of our surrogate potential energy surface. After excitation to the first excited singlet state, continuous steepest descent converges to a minimizer of $\hat{\mathbf{x}}^1 = (101, 14.4, 14.4)$. Upon relaxation, the effects of thermal fluctuations and molecular vibrations again either send the molecule back to a *cis* geometry or toward *trans*. Fifty different reaction paths are shown in Figure 5.

The simulation finds several different ground state local minima, but each has values sufficiently close to 0 or 180 for x_1. The discrepancy in the stable ground state geometries and $\hat{\mathbf{x}}^1$

dx.doi.org/10.1021/ct5004669 | J. Chem. Theory Comput. 2014, 10, 2942−2949

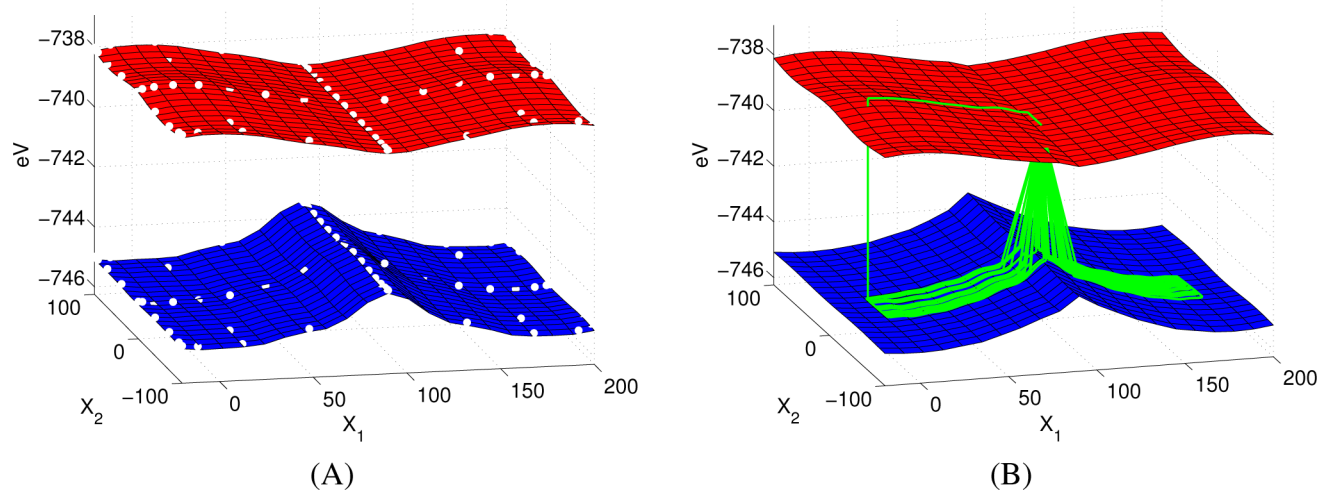

Figure 4. (A) Ground and first excited state potential energy surfaces approximated with $k = 4$. The white points on the potential energy surfaces are the sparse grid points. (B) 50 simulation reaction paths on potential energy surfaces approximated with $k = 5$.

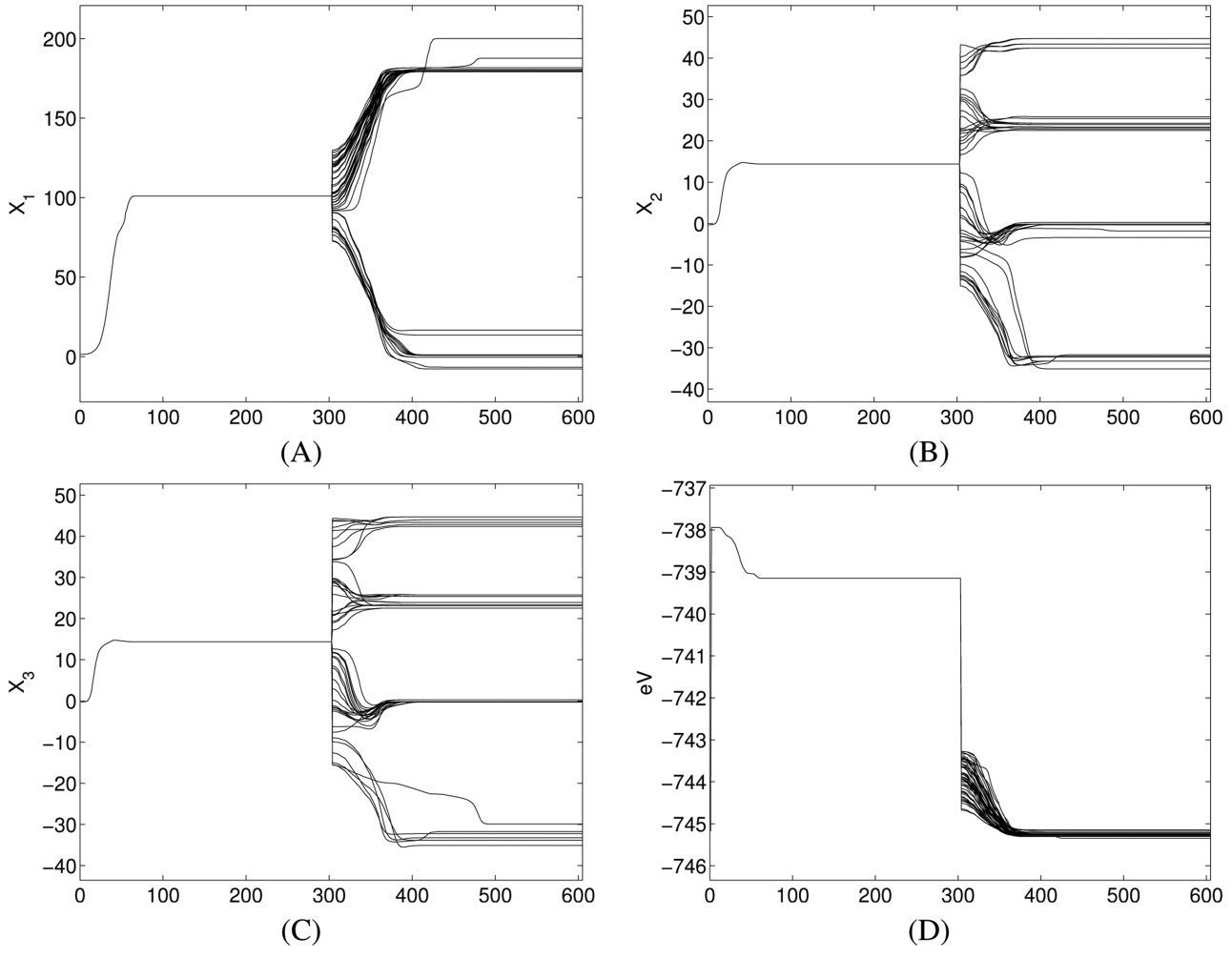

Figure 5. Simulation 3 results for 2-butene: (A) reaction paths for design variable x_1, (B) reaction paths for design variable x_2, (C) reaction paths for design variable x_3, (D) energies for reaction paths.

between the two-dimensional simulations and the three-dimensional simulation can be explained by the inclusion of x_3. By including a third design variable, and thus increasing the dimension of our problem, we get a more complete picture of the reaction path, but we also lose some degree of interpolation accuracy from the increase in dimension d (see ref 73 for explicit error bounds). As in the two-dimensional simulations, however, the nested structure of sparse grids would allow us to easily construct approximate potential energy surfaces with $k = 6$ if more accuracy were needed.

dx.doi.org/10.1021/ct5004669 | J. Chem. Theory Comput. 2014, 10, 2942−2949

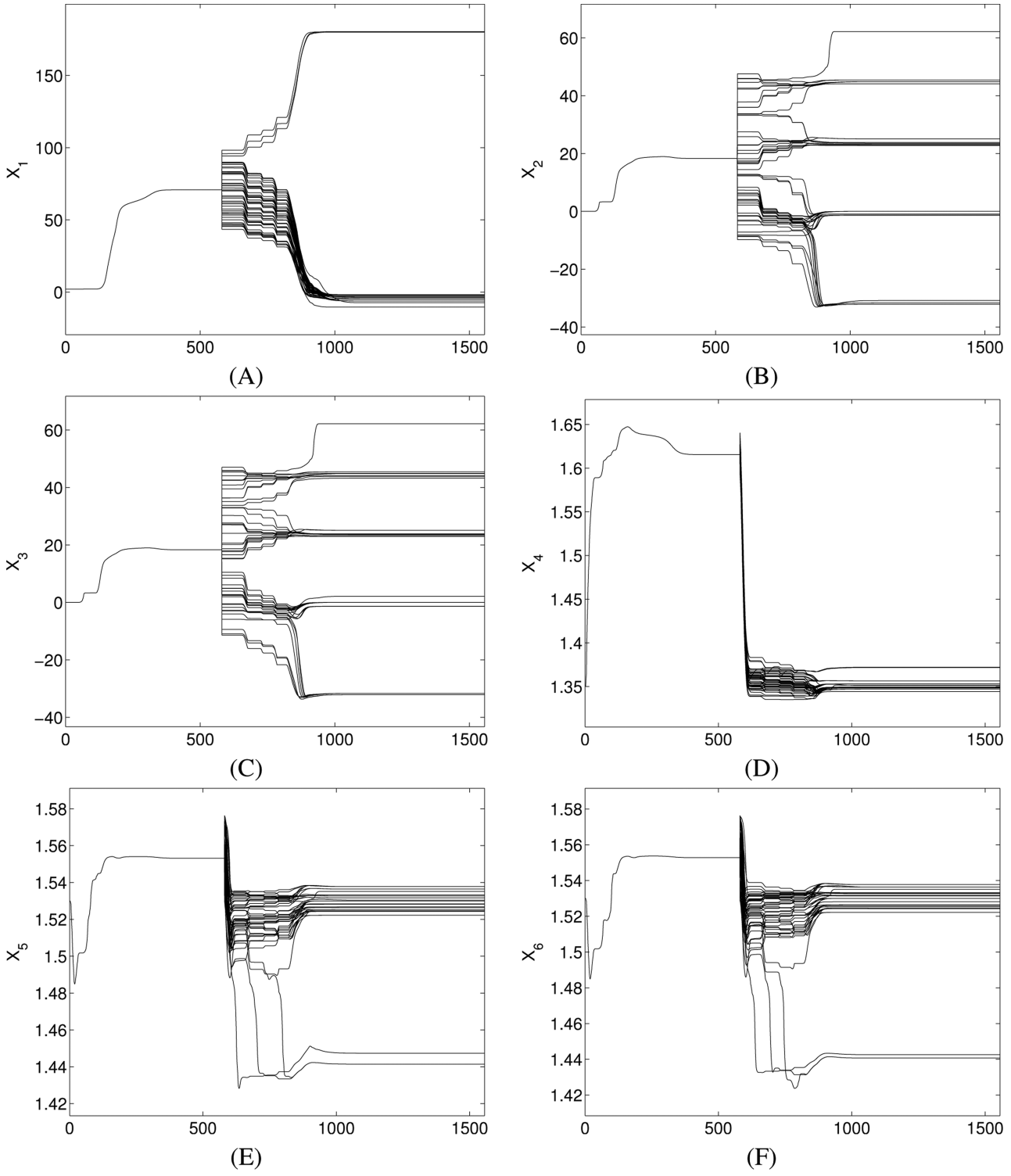

Figure 6. Simulation 4 results for 2-butene: (A) reaction paths for design variable x_1, (B) reaction paths for design variable x_2, (C) reaction paths for design variable x_3, (D) reaction paths for design variable x_4, (E) reaction paths for design variable x_5, (F) reaction paths for design variable x_6.

3.2.4. Simulation 4: d = 6, k = 5. Finally, we include the three carbon−carbon bonds for a total of six degrees of freedom. Simulations begin in the ground state at the local minimum $\mathbf{x}$ = (2.2, 0.0, 0.0, 1.35, 1.53, 1.53) corresponding to the *cis* geometry and are excited to the first electronic state. Continuous steepest descent converges to a minimum of $\hat{\mathbf{x}}^1$ = (70.8, 18.3, 18.3, 1.62, 1.55, 1.55) on the first excited state PES and 50 reaction paths are reinitialized on the ground state. Reaction paths for all six degrees of freedom are shown in Figure 6.

As with simulation 3, the simulation converges to several local minima. The dihedral angle x_1 behaves as expected, with trajectories converging sufficiently close to 0 or 180. Dihedral angles x_2 and x_3 do not vary much on the excited state PES, but the simulated effects of randomness send the trajectories toward different local minima. The reaction paths for x_4 show

dx.doi.org/10.1021/ct5004669 | J. Chem. Theory Comput. 2014, 10, 2942−2949

that the $C^2{=}C^3$ bond length varies by almost 0.3 during the reaction, lengthening to 1.65 on the excited state PES and shrinking back to approximately 1.35 on the ground state PES. The single bond lengths x_5 and x_6 vary as well, but by no more than 0.05 for most simulations. For three reaction paths both of these coordinates converge to much shorter bond lengths approximately equal to 1.44. Energy paths resemble those shown in Figure 5D for simulation 3 and are not shown for this simulation.

4. CONCLUSIONS

In this paper, we have presented a method for reaction path following on potential energy surfaces approximated with sparse interpolation.[1,73,74] Sparse interpolation efficiently improves the ratio of invested storage and computing time to approximation accuracy, so our method allows one to increase the degrees of freedom in molecule reaction path following simulations. The one-time computational cost of the method comes from the number of electronic structure calculations required by the sparse interpolation algorithm. However, these calculations are independent of each other and are thus easily parallelizable. While the calculations can still be time-consuming, once they are performed the construction and evaluation of the interpolatory surrogate model is computationally inexpensive.

Our surrogate model approach allows one to continuously follow entire reaction paths, a task that is too computationally burdensome to perform with the actual potential energy surfaces. As a representative example, we have successfully simulated reaction paths for the isomerization of 2-butene and shown how easily one can obtain increasingly accurate approximations of the potential energy surfaces. While 2-butene is relatively small molecule, we are currently studying reactions of larger molecules.

■ ASSOCIATED CONTENT

Supporting Information

Mathematical details of Smolyak's algorithm[1,73,74] and *GAUSSIAN 09*[103] input details for 2-butene calculations. This material is available free of charge via the Internet at http://pubs.acs.org/.

■ AUTHOR INFORMATION

Corresponding Author

*Phone: 919-515-7163. Fax: 919-515-3798. Email: tim_kelley@ncsu.edu

Notes

The authors declare no competing financial interest.

■ ACKNOWLEDGMENTS

This work has been partially supported by Army Research Office Grant W911NF-11-1-0367, and NSF Grants CDI-0941253, DMS-1406349, SI2-SSE-1339844, and 1127914 to the Statistical and Applied Mathematical Sciences Institute. Any opinions, findings, and conclusions or recommendations expressed in this material are those of the author(s) and do not necessarily reflect the views of the Army Research Office or the National Science Foundation. The authors thank the reviewers for their helpful comments.

■ REFERENCES

(1) Smolyak, S. *Soviet Math. Dokl.* **1963**, *4*, 240−243.
(2) Wales, D. J. *Energy Landscapes*; Cambridge University Press: Cambridge, U.K., 2003; p 301.
(3) Laio, A.; Parrinello, M. *Proc. Natl. Acad. Sci. U.S.A.* **2002**, *99*, 12562−12566.
(4) Wu, Y.; Schmitt, J. D.; Car, R. *J. Chem. Phys.* **2004**, *121*, 1193−1200.
(5) Ensing, B.; Laio, A.; Parrinello, M.; Klein, M. L. *J. Phys. Chem. B* **2005**, *109*, 6676−6687.
(6) Maeda, S.; Ohno, K. *J. Phys. Chem. A* **2005**, *109*, 5742−5753.
(7) Ohno, K.; Maeda, S. *Chem. Phys. Lett.* **2004**, *384*, 277−282.
(8) Maeda, S.; Watanabe, Y.; Ohno, K. *Chem. Phys. Lett.* **2005**, *414*, 265−270.
(9) Ohno, K.; Maeda, S. *Phys. Scr.* **2008**, *78*, 058122.
(10) Burger, S. K.; Ayers, P. W. *J. Chem. Theory Comput.* **2010**, *6*, 1490−1497.
(11) Burger, S. K.; Liu, Y.; Sarkar, U.; Ayers, P. W. *J. Chem. Phys.* **2009**, *130*, 024103.
(12) Dey, B. K.; Janicki, M. R.; Ayers, P. W. *J. Chem. Phys.* **2004**, *121*, 6667−6679.
(13) Dey, B. K.; Bothwell, S.; Ayers, P. W. *J. Math. Chem.* **2006**, *41*, 1−25.
(14) Liu, Y.; Burger, S. K.; Dey, B. K.; Sarkar, U.; Janicki, M. R.; Ayers, P. W. In *Quantum Biochemistry*; Matta, C. F., Ed.; Wiley-VCH: Boston, 2010; pp 171−195.
(15) Grubmüller, H. *Phys. Rev. E* **1995**, *52*, 2893−2906.
(16) Müller, E. M.; de Meijere, A.; Grubmüller, H. *J. Chem. Phys.* **2002**, *116*, 897−905.
(17) Cerjan, C. J.; Miller, W. H. *J. Chem. Phys.* **1981**, *75*, 2800−2806.
(18) Bell, S.; Crighton, J. S. *J. Chem. Phys.* **1984**, *80*, 2464−2475.
(19) Elber, R.; Karplus, M. *Chem. Phys. Lett.* **1987**, *139*, 375−380.
(20) Schlegel, H. B. *J. Chem. Soc. Faraday Trans.* **1994**, *90*, 1569−1574.
(21) Heidrich, D., Ed. *The Reaction Path in Chemistry: Current Approaches and Perspectives*; Kluwer Academic Publishers: Dordrecht, 1995; pp 1−294.
(22) Ayala, P. Y.; Schlegel, H. B. *J. Chem. Phys.* **2001**, *107*, 375−384.
(23) Schlegel, H. B. *J. Comput. Chem.* **2003**, *24*, 1514−1527.
(24) Hratchian, H. P.; Schlegel, H. B. In *Theory and Applications of Computational Chemistry: The First Forty Years*, 1st ed.; Dykstra, C., Frenking, G., Kim, K., Scuseria, G., Eds.; Elsevier BV: Amsterdam, 2005; Chapter 10, pp 195−249.
(25) Sheppard, D.; Terrell, R.; Henkelman, G. *J. Chem. Phys.* **2008**, *128*, 1−10.
(26) Hratchian, H. P.; Frisch, M. J. *J. Chem. Phys.* **2011**, *134*, 204103.
(27) Birkholz, A. B.; Schlegel, H. B. *Theor. Chem. Acc.* **2012**, *131*, 1170.
(28) Bofill, J. M.; Quapp, W.; Caballero, M. *Chem. Phys. Lett.* **2013**, *583*, 203−208.
(29) Boggio-Pasqua, M.; Burmeister, C. F.; Robb, M. a.; Groenhof, G. *Phys. Chem. Chem. Phys.* **2012**, *14*, 7912−7928.
(30) Mendive-Tapia, D.; Vacher, M.; Bearpark, M. J.; Robb, M. a. *J. Chem. Phys.* **2013**, *139*, 044110.
(31) Jiang, C.; Xie, R.; Li, F.; Allen, R. E. *Chem. Phys. Lett.* **2009**, *474*, 263−267.
(32) Allen, R. E.; Dumitrica, T.; Torralva, B. R. In *Ultrafast Physical Processes in Semiconductors*; Tsen, K. T., Ed.; Academic Press: San Diego, 2001; Chapter 7, pp 315−388.
(33) Warshel, A. *Nature* **1976**, *260*, 679−683.
(34) Tully, J. C.; Preston, R. K. *J. Chem. Phys.* **1971**, *55*, 562−572.
(35) Tully, J. C. *J. Chem. Phys.* **1990**, *93*, 1061−1071.
(36) Tully, J. C. *Int. J. Quantum Chem.* **1991**, *40*, 299−309.
(37) Tully, J. C. *Faraday Discuss.* **1998**, *110*, 407−419.
(38) Tully, J. C. *J. Chem. Phys.* **2012**, *137*, 22A301.
(39) Warshel, A.; Levitt, M. *J. Mol. Biol.* **1976**, *103*, 227−249.
(40) Liu, H.; Lu, Z.; Cisneros, G. A.; Yang, W. *J. Chem. Phys.* **2004**, *121*, 697−706.
(41) Xie, L.; Liu, H.; Yang, W. *J. Chem. Phys.* **2004**, *120*, 8039−8052.
(42) Hu, H.; Yang, W. *Annu. Rev. Phys. Chem.* **2008**, *59*, 573−601.

(43) Cisneros, G. A.; Liu, H.; Zhang, Y.; Yang, W. *J. Am. Chem. Soc.* **2003**, *125*, 10384−10393.
(44) Cisneros, G. A.; Liu, H.; Lu, Z.; Yang, W. *J. Chem. Phys.* **2005**, *122*, 114502.
(45) Dou, Y.; Allen, R. E. *J. Chem. Phys.* **2003**, *119*, 10658−10666.
(46) Dou, Y.; Torralva, B. R.; Allen, R. E. *J. Mod. Opt.* **2003**, *50*, 2615−2643.
(47) Albu, T. V.; Corchado, C.; Truhlar, D. G. *J. Phys. Chem. A* **2001**, *105*, 8465−8487.
(48) Higashi, M.; Truhlar, D. G. *J. Chem. Theory Comput.* **2008**, *4*, 790−803.
(49) Lin, H.; Pu, J.; Albu, T. V.; Truhlar, D. G. *J. Phys. Chem. A* **2004**, *108*, 4112−4124.
(50) Lin, H.; Zhao, Y.; Tishchenko, O.; Truhlar, D. G. *J. Chem. Theory Comput.* **2006**, *2*, 1237−1254.
(51) Tishchenko, O.; Truhlar, D. G. *J. Phys. Chem. A* **2006**, *110*, 13530−13536.
(52) Tishchenko, O.; Truhlar, D. G. *J. Chem. Phys.* **2009**, *130*, 024105.
(53) Martinez, T. J.; Levine, R. D. *J. Chem. Soc. Faraday Trans.* **1997**, *93*, 941−947.
(54) Ben-Nun, M.; Queenneville, J.; Martinez, T. J. *J. Phys. Chem. A* **2000**, *104*, 5161−5175.
(55) Levine, B. G.; Coe, J. D.; Virshup, A. M.; Martnez, T. J. *Chem. Phys.* **2008**, *347*, 3−16.
(56) Barbatti, M.; Granucci, G.; Persico, M.; Ruckenbauer, M.; Vazdar, M.; Eckert-Maksić, M.; Lischka, H. *J. Photochem. Photobiol. A: Chem.* **2007**, *190*, 228−240.
(57) Barbatti, M.; Ruckenbauer, M.; Plasser, F.; Pittner, J.; Granucci, G.; Persico, M.; Lischka, H. *Wiley Interdiscip. Rev.: Comput. Mol. Sci.* **2014**, *4*, 26−33.
(58) Takatsuka, K.; Yonehara, T. *Phys. Chem. Chem. Phys.* **2011**, *13*, 4987−5016.
(59) Yonehara, T.; Hanasaki, K.; Takatsuka, K. *Chem. Rev.* **2012**, *112*, 499−542.
(60) Prenter, P. M. *Splines and Variational Methods*; Wiley: New York, 1975; Vol. *56*; pp 1−334.
(61) Sathyamurthy, N. *J. Chem. Phys.* **1975**, *63*, 464−473.
(62) Mokrauer, D. S.; Kelley, C. T.; Bykhovski, A. *IEEE Trans. Nanotechnol.* **2011**, *10*, 70−74.
(63) Patrício, M.; Santos, J. L.; Patrcio, F.; Varandas, A. J. C. *J. Math. Chem.* **2013**, *51*, 1729−1746.
(64) Ischtwan, J.; Collins, M. A. *J. Chem. Phys.* **1994**, *100*, 8080−8088.
(65) Collins, M. A. *Theor. Chem. Acc.* **2002**, *108*, 313−324.
(66) Godsi, O.; Evenhuis, C. R.; Collins, M. A. *J. Chem. Phys.* **2006**, *125*, 104105.
(67) Maisuradze, G. G.; Thompson, D. L.; Wagner, A. F.; Minkoff, M. *J. Chem. Phys.* **2003**, *119*, 10002.
(68) Maisuradze, G. G.; Kawano, A.; Thompson, D. L.; Wagner, A. F.; Minkoff, M. *J. Chem. Phys.* **2004**, *121*, 10329−10338.
(69) Mokrauer, D. S.; Kelley, C. T.; Bykhovski, A. *9th Int. Symp. Distributed Comput. Appl. Bus. Eng. Sci.* **2010**, 1−4.
(70) Mokrauer, D. S. Interpolatory Surrogate Models for Light-Induced Transition Dynamics. Ph.D. thesis, North Carolina State University, Raleigh, NC, 2012.
(71) Mokrauer, D. S.; Kelley, C. T.; Bykhovski, A. *J. Algorithms Comp. Technol.* **2012**, *6*, 577−592.
(72) Mokrauer, D. S.; Kelley, C. T. *Optim. Methods Softw.* **2014**, *29*, 264−273.
(73) Barthelmann, V.; Novak, E.; Ritter, K. *Adv. Comp. Math.* **2000**, *12*, 273−288.
(74) Judd, K. L.; Maliar, L.; Maliar, S.; Valero, R. *Smolyak Method for Solving Dynamic Economic Models: Lagrange Interpolation, Anisotropic Grid and Adaptive Domain*; Working Paper 19326, 2013; pp 1−47, http://www.nber.org/papers/w19326 (accessed Jan. 5, 2014).
(75) Gradinaru, V. *Computing* **2007**, *80*, 1−22.
(76) Griebel, M.; Hamaekers, J. *ESAIM: Math. Modell. Numer. Anal.* **2007**, *41*, 215−247.
(77) Rodríguez, J. I.; Thompson, D. C.; Ayers, P. W.; Köster, A. M. *J. Chem. Phys.* **2008**, *128*, 224103.
(78) Rodriguez, J. I.; Thompson, D. C.; Anderson, J. S. M.; Thomson, J. W.; Ayers, P. W. *J. Phys. A: Math. Theor.* **2008**, *41*, 365202.
(79) Avila, G.; Carrington, T. *J. Chem. Phys.* **2009**, *131*, 174103.
(80) Avila, G.; Carrington, T. *J. Chem. Phys.* **2011**, *135*, 064101.
(81) Avila, G.; Carrington, T. *J. Chem. Phys.* **2011**, *134*, 054126.
(82) Avila, G.; Carrington, T. *J. Chem. Phys.* **2012**, *137*, 174108.
(83) Avila, G.; Carrington, T. *J. Chem. Phys.* **2013**, *139*, 134114.
(84) Novak, E.; Ritter, K. *Constructive Approximation* **1999**, *15*, 499−522.
(85) Bungartz, H.-J.; Griebel, M. *Acta Numerica* **2004**, *13*, 1−123.
(86) Wasilkowski, G. W.; Wozniakowski, H. *J. Complexity* **1995**, *11*, 1−56.
(87) Minyaev, R. M. *Int. J. Quantum Chem.* **1994**, *49*, 105−127.
(88) Luo, X.-L.; Kelley, C. T.; Liao, L.-Z.; Tam, H. W. *J. Optim. Theory Appl.* **2009**, *140*, 265−286.
(89) Courant, R. *Bull. Am. Math. Soc.* **1943**, *49*, 1−43.
(90) *MATLAB*, Version 8.3.0 (R2014a); The MathWorks, Inc.: Natick, MA, 2014.
(91) Shampine, L. F.; Reichelt, M. W. *SIAM J. Sci. Comput.* **1997**, *18*, 1−22.
(92) Hoffmann, R. *J. Chem. Phys.* **1963**, *39*, 1397−1412.
(93) Beringhelli, T.; Gavezzotti, A.; Simonetta, M. *J. Mol. Struct.* **1972**, *12*, 333−342.
(94) Hart, W. J. V. D. *J. Am. Soc. Mass Spectrom.* **1999**, *10*, 575−586.
(95) Palmer, I. J.; Ragazos, I. N.; Bernardi, F.; Olivucci, M.; Robb, M. A. *J. Am. Chem. Soc.* **1993**, *115*, 673−682.
(96) Woolard, D. L.; Brown, R.; Pepper, M.; Kemp, M. *Proc. IEEE* **2005**, *93*, 1722−1743.
(97) Stephens, P. J.; Devlin, F. J.; Chabalowski, C. F.; Frisch, M. J. *J. Phys. Chem.* **1994**, *98*, 11623−11627.
(98) Kim, K.; Jordan, K. D. *J. Phys. Chem.* **1994**, *98*, 10089−10094.
(99) Stevens, W. J.; Basch, H.; Krauss, M. *J. Chem. Phys.* **1984**, *81*, 6026−6033.
(100) Stevens, W. J.; Krauss, M.; Basch, H.; Jasien, P. G. *Can. J. Chem.* **1992**, *70*, 612−630.
(101) Cundari, T. R.; Stevens, W. J. *J. Chem. Phys.* **1993**, *98*, 5555−5565.
(102) Runge, E.; Gross, E. K. U. *Phys. Rev. Lett.* **1984**, *52*, 997−1000.
(103) Frisch, M. J.; Trucks, G. W.; Schlegel, H. B.; Scuseria, G. E.; Robb, M. A.; Cheeseman, J. R.; Scalmani, G.; Barone, V.; Mennucci, B.; Petersson, G. A.; Nakatsuji, H.; Caricato, M.; Li, X.; Hratchian, H. P.; Izmaylov, A. F.; Bloino, J.; Zheng, G.; Sonnenberg, J. L.; Hada, M.; Ehara, M.; Toyota, K.; Fukuda, R.; Hasegawa, J.; Ishida, M.; Nakajima, T.; Honda, Y.; Kitao, O.; Nakai, H.; Vreven, T.; Montgomery Jr., J. A.; Peralta, J. E.; Ogliaro, F.; Bearpark, M.; Heyd, J. J.; Brothers, E.; Kudin, K. N.; Staroverov, V. N.; Kobayashi, R.; Normand, J.; Raghavachari, K.; Rendell, A.; Burant, J. C.; Iyengar, S. S.; Tomasi, J.; Cossi, M.; Rega, N.; Millam, J. M.; Klene, M.; Knox, J. E.; Cross, J. B.; Bakken, V.; Adamo, C.; Jaramillo, J.; Gomperts, R.; Stratmann, R. E.; Yazyev, O.; Austin, A. J.; Cammi, R.; Pomelli, C.; Ochterski, J. W.; Martin, R. L.; Morokuma, K.; Zakrzewski, V. G.; Voth, G. A.; Salvador, P.; Dannenberg, J. J.; Dapprich, S.; Daniels, A. D.; Farkas, O.; Foresman, J. B.; Ortiz, J. V.; Cioslowski, J.; Fox, D. J. *Gaussian 09*, Revision A.1; Gaussian, Inc.: Wallingford, CT, 2009.
(104) Nance, J.; Kelley, C. T. *A Sparse Interpolation Algorithm for Dynamical Simulations in Computational Chemistry* **2014**, submitted to SIAM J. Sci. Comput.